Theory and Performance of a Power-Combining Multiple-Device Ladder Amplifier

SHIGEJI NOGI, KIYOSHI FUKUI, MEMBER, IEEE, AND SATOSHI TANAKA

Abstract—**This paper presents a detailed discussion on the microwave power amplification using a multiple-device ladder structure which is essentially an array of diode-mount-pairs in a rectangular waveguide cavity. For both transmission and reflection types, the capability of perfect combining of available powers from each component device and available input signal power is analytically described. A power flow distribution along the structure is also described to interpret the power-combining mechanism. Amplifier characteristics are studied through numerical analysis and well confirmed by experiments on X-band amplifiers with up to eight Gunn diodes.**

I. Introduction

IN RECENT YEARS, many power-combining techniques for microwave and millimeter-wave solid-state power sources have been proposed. They were well reviewed by K. J. Russell [1] in 1979 and by K. Chang and C. Sun [2] in 1983.

The authors proposed the oscillator with a very simple multiple-device structure, that is, a microwave ladder structure which is essentially an array of diode-mount-pairs in a rectangular waveguide, and gave a detailed discussion on the power-combining mechanism and the stable operation at the desired mode [3]–[5]. Various multiple-device oscillators using a rectangular waveguide cavity were also reported by several authors [6]–[10]. It is mentioned in [2], that the combiners of such a type are particularly favorable in the millimeter-wave frequency range.

In the multiple-device ladder oscillator, power-combining operation can be realized by the design which makes the RF voltage amplitude at each diode-mount-pair equal to that for available power generation. This fact suggests the possibility of amplifier-use of the multiple-device structures capable of combining both input power and available powers of each active device.

This paper deals with power amplification using the multiple-device ladder structure. Both transmission-type and reflection-type amplifiers are treated, and their power-combining designs and amplifier characteristics are clarified first by theoretical analysis based on their equivalent circuit, and second by experiment. It is noted that the analytical method in this paper can be applicable to every multiple-device power amplifier of the rectangular waveguide cavity type, because such an amplifier can be commonly represented by the equivalent circuit adopted in this paper. In Section II, we discuss analytically the transmission-type power amplifier, derive the power-combining design formula together with the equations for power flow distribution along the ladder structure, and we present the numerical results for both output versus input power characteristic and frequency response. Section III is devoted to a similar discussion on the reflection-type power amplifier. In Section IV, we give the experimental results on the characteristics of power amplifiers of both types with up to four diode-mount-pairs.

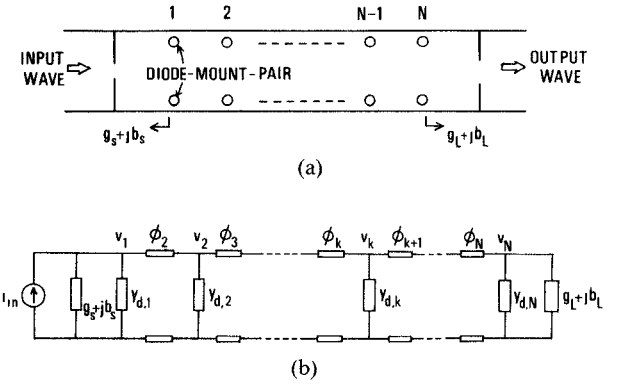

Fig. 1. Transmission-type power amplifier with a multiple-device ladder structure. (a) Construction. (b) Equivalent-circuit representation.

II. Transmission-Type Power Amplifier

A. Circuit Configuration and its Equivalent Representation

A transmission-type power amplifier is constructed by setting coupling windows at both ends of a multiple-device ladder structure as shown in Fig. 1(a). An input wave is introduced through the left window and an output wave extracted through the right one. Assuming that the waveguide can propagate only in the dominant (TE_{10}) mode, the equivalent representation is given by Fig. 1(b). In this figure, $y_{dk} = g_k + jb_{pk}$ is the admittance of the kth diode-mount-pair, which includes the effect of the mounting structure and package parasitics, and $y_s = g_s + jb_s$ is the source admittance looking left from the first mount-pair, while $y_L = g_L + jb_L$ is the load admittance looking right

Manuscript received June 17, 1985; revised October 25, 1985. This work was supported in part by a Research Grant from Hōsō-Bunka (Broadcasting Culture) Foundation.

S. Nogi and K. Fukui are with the Department of Electronics, Okayama University, Okayama 700, Japan.

S. Tanaka was with the Department of Electronics, Okayama University, Okayama 700, Japan. He is now with Visual Information Systems Development Center, Matsushita Electric Industrial Company, Ltd., Osaka 570, Japan.

IEEE Log Number 8406860.

from the Nth mount-pair (all the admittances are normalized by the characterictic admittance Y_0 of the waveguide). $\phi_2, \phi_3, \cdots, \phi_N$ denote the electrical length of the corresponding waveguide portions. The input signal is provided by the current source

$$i_{in} = Y_0 V_{in} e^{j\omega t} \tag{1}$$

whose available power is given by

$$P_{in,a} = Y_0 V_{in}^2/(8g_s). \tag{2}$$

B. Maximum Output Power

Putting $v_k = V_k e^{j(\omega t + \psi_k)}$, we have the circuit equation from Fig. 1(b) as

$$b_{tk} V_{k-1} \sin \psi_{k,k-1} + (g_s \delta_{k1} + g_k + g_L \delta_{kN}) V_k - b_{t,k+1} V_{k+1} \sin \psi_{k+1,k} = V_{in} \cos \psi_1 \cdot \delta_{k1} \tag{3a}$$

$$b_{tk} V_{k-1} \cos \psi_{k,k-1} + b_k V_k + b_{t,k+1} V_{k+1} \cos \psi_{k+1,k} = -V_{in} \sin \psi_1 \cdot \delta_{k1}, \qquad k = 1, 2, \cdots, N \tag{3b}$$

where

$$\psi_{k,k-1} = \psi_k - \psi_{k-1} \tag{4a}$$

$$b_k = \begin{cases} b_s + b_{p1} - \cot \phi_2, & k = 1 \\ -\cot \phi_k + b_{pk} - \cot \phi_{k+1}, & 2 \leqq k \leqq N-1 \\ -\cot \phi_N + b_{pN} + b_L, & k = N \end{cases} \tag{4b}$$

$$b_{tk} = \begin{cases} \operatorname{cosec} \phi_k, & 2 \leqq k \leqq N \\ 0, & k = 1,\ N+1 \end{cases} \tag{4c}$$

and δ_{kl} is the Kronecker delta.

The negative conductance g_k is assumed to be dependent on the voltage amplitude V_k. The power generated by g_k is given by

$$P_k = -(Y_0/2) g_k(V_k) V_k^2 \tag{5}$$

which reaches the maximum value at $V_k = V_{k,\mathrm{opt}}$ and $g_k = g_k(V_{k,\mathrm{opt}})$ $(\equiv g_{k,\mathrm{opt}})$[1] such as

$$P_{k,\max} = -\frac{Y_0}{2} g_{k,\mathrm{opt}} V_{k,\mathrm{opt}}^2 \ (\equiv P_{d,k}), \tag{6}$$

The output power of the amplifier is obtained from (3a) as

$$P_0 = \frac{1}{2} g_L Y_0 V_N^2 = \frac{1}{2} Y_0 \left(V_1 V_{in} \cos \psi_1 - g_s V_1^2 \right) - \frac{1}{2} Y_0 \sum_{k=1}^{N} g_k V_k^2 \tag{7}$$

which states that P_0 is equal to the sum of the power effectively injected to the amplifier and the total power yielded by all the diodes.

[1]At the maximum power generation, $dP_k/dV_k = 0$ leads to

$$dg_k/dV_k|_{V_k = V_{k,\mathrm{opt}}} = -2 g_{\mathrm{opt}}/V_{k,\mathrm{opt}}.$$

For a given available input power, the output power of the amplifier takes the maximum value (from (7), (6), and (2)) given by

$$P_{0,\max} = P_{in,a} + \sum_{k=1}^{N} P_{d,k} \tag{8}$$

when

$$\psi_1 = 0 \tag{9a}$$

$$V_k = V_{k,\mathrm{opt}}, \qquad 1 \leqq k \leqq N \tag{9b}$$

and

$$V_{in} = \frac{4 P_{in,a}}{Y_0 V_{1,\mathrm{opt}}}. \tag{9c}$$

Equation (8) shows that the transmission-type amplifier is able to combine the available power of the input signal and all of those of each diode-mount-pair perfectly. The optimum source conductance $g_{s,\mathrm{opt}}$ is given from (2), (6), and (9c) as

$$g_{s,\mathrm{opt}} = -g_{1,\mathrm{opt}} \frac{P_{in,a}}{P_{d,1}} \tag{10}$$

and the optimum load conductance $g_{L,\mathrm{opt}}$ is obtained from (6)–(8) and (9b) as

$$g_{L,\mathrm{opt}} = -g_{N,\mathrm{opt}} \frac{P_{in,a} + \sum_{k=1}^{N} P_{d,k}}{P_{d,N}}. \tag{11}$$

C. Optimum Design for Perfect Power Combining

In the following, all the parameters of diode-mount-pairs are assumed to be equal to each other, for simplicity, and the subscript k in g_k, b_{pk}, $P_{d,k}$, $V_{k,\mathrm{opt}}$, and $g_{k,\mathrm{opt}}$ is omitted. For the perfect power-combining operation, we obtain from (3), (9), and (10)

$$\left\{ \frac{P_{in,a}}{P_d} + (k-1) \right\} g_{\mathrm{opt}} = b_{tk} \sin \psi_{k,k-1} \tag{12a}$$

$$\sum_{l=1}^{k-1} (-1)^{k-l} b_l = b_{tk} \cos \psi_{k,k-1}, \qquad 2 \leqq k \leqq N. \tag{12b}$$

Elimination of $\psi_{k,k-1}$ from these equations yields

$$\left\{ \frac{P_{in,a}}{P_d} + (k-1) \right\}^2 g_{\mathrm{opt}}^2 + \left\{ \sum_{l=1}^{k-1} (-1)^{k-l} b_l \right\}^2 = b_{tk}^2, \qquad 2 \leqq k \leqq N. \tag{13}$$

On the other hand, we have from (3b), (9a), and (9b)

$$\sum_{k=1}^{N} (-1)^k b_k = 0. \tag{14}$$

When any one of b_s, ϕ_2, $\phi_3, \cdots, \phi_N$, and b_L is given, the remainder can be determined by use of the N equations of

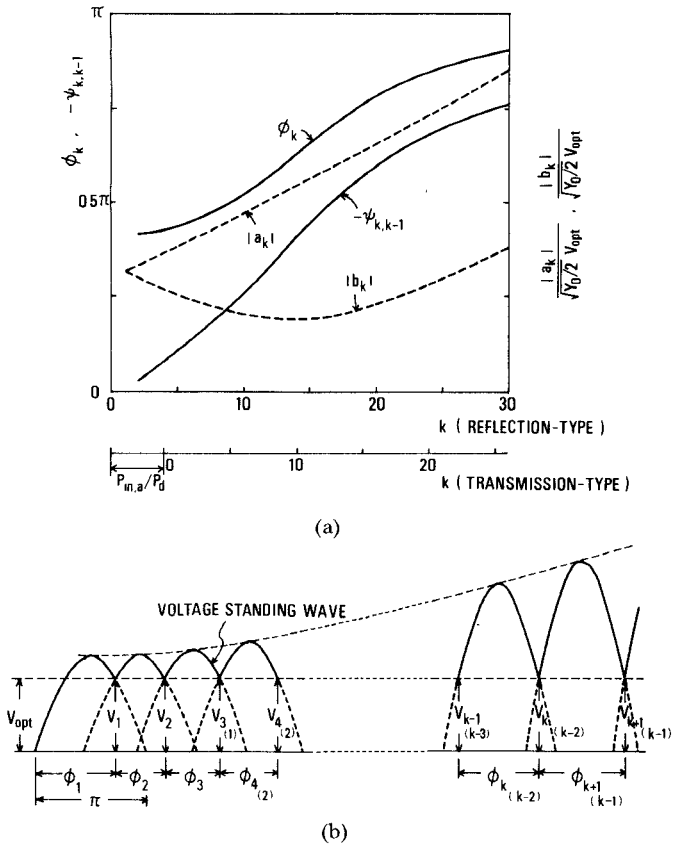

Fig. 2. Power-combining operation. (a) Distribution of ϕ_k, $\psi_{k,k-1}$, $|a_k|$, and $|b_k|$ along the ladder structure ($b_p = -1.5$, $g_{opt} = -0.08$). (b) Voltage standing-wave pattern for reflection amplifier. For transmission amplifier, take the numbers in the parentheses as the subscripts in V_k and ϕ_k (the case of $P_{in,a}/P_d = 2$ is shown as an example).

(13) and (14). We obtain from (13), (4b), and (4c)

$$-\cot\phi_k = \begin{cases} \dfrac{1}{2(b_s+b_p)}\left[1-(b_s+b_p)^2-\left\{\dfrac{P_{in,a}}{P_d}+(k-1)\right\}^2 g_{opt}^2\right], & \text{for even } k \\ \dfrac{1}{-2b_s}\left[1-b_s^2-\left\{\dfrac{P_{in,a}}{P_d}+(k-1)\right\}^2 g_{opt}^2\right], & \text{for odd } k\ (k \geqq 3) \end{cases} \tag{15}$$

and from (14) and (4b)

$$\begin{aligned} -b_s + b_L &= 0, \quad \text{for even } N \\ b_s + b_p + b_L &= 0, \quad \text{for odd } N. \end{aligned} \tag{16}$$

Especially, when we take as

$$b_s = -b_p/2 \tag{17}$$

(15) and (16) are simplified as

$$-\cot\phi_k = \frac{1}{b_p}\left[1-\left(\frac{b_p}{2}\right)^2-\left\{\frac{P_{in,a}}{P_d}+(k-1)\right\}^2 g_{opt}^2\right], \quad \text{for any } k \tag{15'}$$

and

$$b_L = -b_p/2 \tag{16'}$$

respectively.

The amplifier design for perfect power combining is given using (15) and (16), or, in their special case, (17), (15′) and (16′), together with (10) and (11). ϕ_k''s are preferably chosen as $0 < \phi_k < \pi$ because the smaller amplifier cavity gives the wider frequency response. For typical g_{opt} and b_p values, the values of ϕ_k and $\psi_{k,k-1}$ obtained by (15′) and (12), respectively, are shown in Fig. 2(a).

D. Traveling Waves in the Cavity

Under the power-combining operation of an amplifier designed using (17), (15′), and (16′), consider a wave traveling toward the output window and one traveling toward the input window between the $(k-1)$th and the kth mount-pairs, and denote these waves by the normal variables defined at the middle of the line ϕ_k as a_k and b_k ($2 \leqq k \leqq N$), respectively. Similarly, a_1 and b_1 are defined just at the left of the first mount-pair, and a_{N+1} and b_{N+1} just at the right of the Nth one.

Using (2) and (9), we have at the left of the first mount-pair of Fig. 1(b)

$$a_1 + b_1 = \sqrt{Y_0/2}\,V_{opt} \tag{18a}$$

$$a_1 - b_1 = \left(1/\sqrt{2Y_0}\right)\left(g_{s,opt} - jb_s\right)Y_0 V_{opt} \tag{18b}$$

which lead to, by use of (10) and (17)

$$\left.\begin{matrix} a_1 \\ b_1 \end{matrix}\right\} = \sqrt{\frac{Y_0}{2}}\,V_{opt}\cdot\frac{1}{2}\left\{\left(1 \mp \frac{P_{in,a}}{P_d}g_{opt}\right) \pm j\frac{b_p}{2}\right\}. \tag{19a}$$

In (19) and the following, the upper and the lower signs correspond to a_k and b_k, respectively. Similarly, we obtain, using (9b), (11) and (16′),

$$\left.\begin{matrix} a_{N+1} \\ b_{N+1} \end{matrix}\right\} = \sqrt{\frac{Y_0}{2}}\,V_{opt}\cdot\frac{1}{2}\left\{\left(1 \mp \left(\frac{P_{in,a}}{P_d}+N\right)g_{opt} \mp j\frac{b_p}{2}\right\}e^{j\psi_N}\right. \tag{19b}$$

and

$$\left.\begin{matrix} a_k \\ b_k \end{matrix}\right\} = \sqrt{\frac{Y_0}{2}}\,V_{opt}\cdot\operatorname{cosec}\phi_k\cdot\sin\frac{\phi_k \mp \psi_{k,k-1}}{2}\cdot e^{j(\psi_{k-1}+\psi_k)/2}, \quad 2 \leqq k \leqq N. \tag{19c}$$

Equation (19c) shows that the voltage standing wave takes a maximum value at the center of every line ϕ_k ($2 \leqq k \leqq N$). We get the expression for the electric powers of the traveling waves by use of (19c), (12), (17), (4), and (15′) together

with (19a) and (19b) as

$$\left.\begin{matrix}|a_k|^2\\ |b_k|^2\end{matrix}\right\} = \frac{Y_0}{8} V_{\text{opt}}^2 \left[\left\{\left(\left(\frac{P_{in,a}}{P_d}+k-1\right)g_{\text{opt}} \mp 1\right\}^2 + \left(\frac{b_{\text{opt}}}{2}\right)^2\right]\right.,$$
$$1 \leqq k \leqq N+1. \quad (20)$$

This equation leads to

$$|a_k|^2 - |b_k|^2 = P_{in,a} + (k-1)P_d, \qquad 1 \leqq k \leqq N+1 \quad (21)$$

which states that the power flow toward the load through the line ϕ_k is equal to the sum of the input available power and those of the diodes up to the $(k-1)$th diode-mount-pair. Equation (21) with $k=1$ also shows that the reflection of the input wave at the input window is cancelled out by the transmission of the wave b_1 through the same window. $|a_k|$ and $|b_k|$ values obtained from (20) are also plotted in Fig. 2(a).

The above analysis leads to the voltage standing wave in the cavity as shown in Fig. 2(b).

E. Stability of the Structure of Optimum Design

In the preceding, all the circuit relations have been developed under the assumption that all the induced RF voltages V_k's are sinusoidal at the frequency of an input signal. So, it should be noted that all the foregoing expressions including the perfect power-combining and the corresponding optimum design formulas are valid not only for a stable amplifier but also for an injection-locked oscillator amplifier.

The subsequent question is, then, whether the ladder structure of optimum design is stable or not. The stability consideration[2] shows that any oscillation mode in the structure of relatively small N cannot grow in the design for not too small $P_{in,a}/P_d$.

In the following sections, some amplifier characteristics such as the input–output relation and frequency response will be discussed primarily for the ladder structure operated as a stable amplifier. However, the discussion of frequency response can be applied also for the case of an injection-locked-type amplifier, as long as the locking range is sufficiently wide as it is in the case for use in power amplification.

F. Input–Output Characteristic and Frequency Response

We consider the characteristic of the transmission-type amplifier, which is designed for perfect power combining in the case that $P_{in,a}$ has a specific value of $P_{in,0}$ at $f(=\omega/2\pi)=f_0$. We can obtain both the output versus input power characteristics and the frequency response of the amplifier with inductive windows designed by use of (17), (15′), and (16′) with $P_{in,a}=P_{in,0}$ through numerical analysis of (3). It is assumed in the analysis that the negative conductance g_k has the voltage dependence given

[2] For the outline of the method of stability analysis, readers are referred to [5].

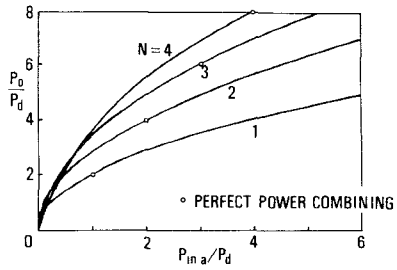

Fig. 3. Output versus input power characteristics of the transmission amplifiers in case of $N=1\sim4$ with the design for $P_{in,0}/P_d=N$ ($g_{\text{opt}}=-0.08$, $b_{p0}=-1.6$).

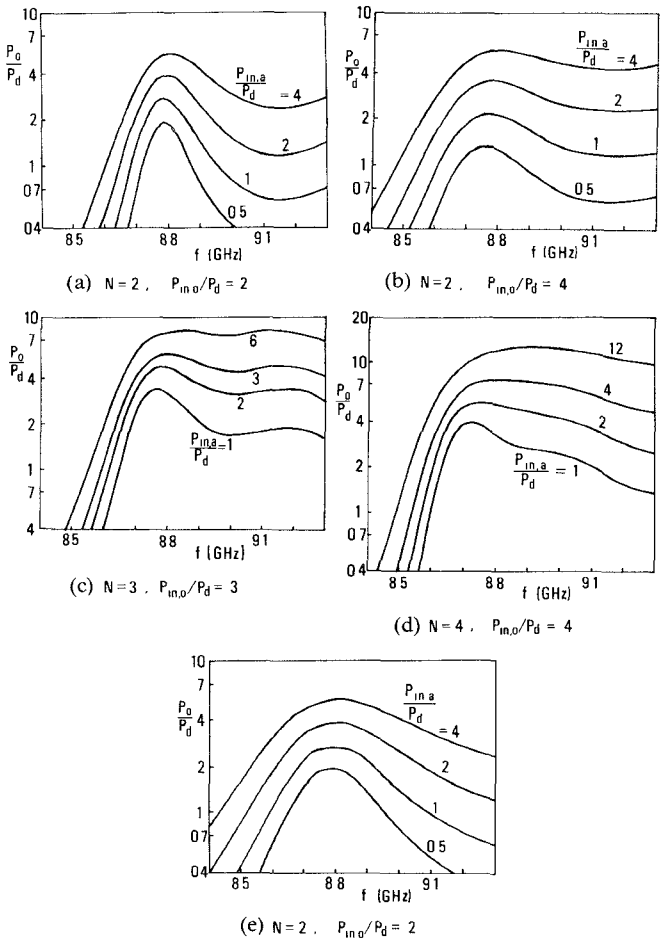

Fig 4. Frequency responses of the transmission amplifiers. The following data are used: $f_0=8.8$ GHZ and $g_{\text{opt}}=-0.08$ together with $b_{p0}=-1.6$ and $b_{p1}=5.1$ for (a)–(d), and $b_{p0}=-0.8$ and $b_{p1}=2.55$ for (e).

by

$$g_k(V_k) = g_{\text{opt}} + \left.\frac{dg_k}{dV_k}\right|_{V_k=V_{\text{opt}}} \cdot (V_k - V_{\text{opt}})$$
$$= g_{\text{opt}}\left\{1-2\left(\frac{V_k}{V_{\text{opt}}}-1\right)\right\} \quad (22)$$

where both g_{opt} and V_{opt} are independent of frequency, and the susceptance b_p has the frequency dependence such as

$$b_p = b_{p0} + b_{p1}(f/f_0 - 1) \quad (23)$$

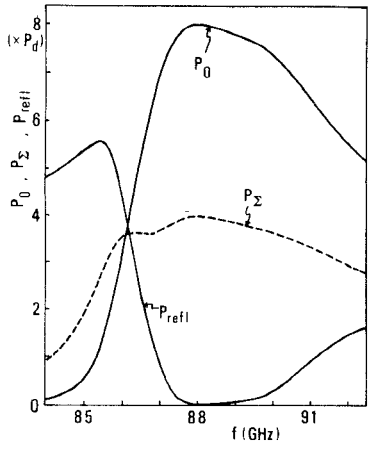

Fig. 5. The output power P_0, the total power yielded by all the diode P_Σ, and the reflected power P_{refl}, of the transmission-type amplifiers for the case of $N=4$ with $P_{in,0}=P_{in,a}=4P_d$.

where b_{p0} and b_{p1} are independent of V_k. The results are shown in Figs. 3 and 4 for typical parameter values of $f_0=8.8$ GHz, $g_{\text{opt}}=-0.08$, $b_{p0}=-1.6$, and $b_{p1}=5.1$ in the cases of $N=1\sim4$. It can be seen from Fig. 3 that the deviation of input power $P_{in,a}$ from $P_{in,0}$ has no considerable effect on the combining efficiency $\eta\equiv P_0/(P_{in,a}+NP_d)$. On the other hand, the frequency response tends to be wider with increasing N,[3] $P_{in,0}$, and $P_{in,a}$ (see Fig. 4(a)–(d)), or decreasing b_p (see Fig. 4(a) and (e)). This result arises because the frequency deviation from f_0 causes the variation of effective input power into the amplifier cavity together with that of the voltage standing wave, which results in the changes of the powers generated by the negative conductances, P_k's in (5).[4] The voltage standing wave varies a relatively small amount in both the case of large $P_{in,0}$, which requires a large aperture of the coupling windows, and that of small b_p, which gives small ϕ_k in (15′). Fig. 5 shows the output power of the amplifier P_0, the total power yielded by all the diodes

$$P_\Sigma=\sum_{k=1}^{N}P_k$$

and the reflected power toward the input source, $P_{\text{refl}}=P_{in,a}+P_\Sigma-P_0$. Numerical analysis indicates that the frequency responses of P_0 and P_{refl} are similar to those of transmitted and reflected power in the linear system which is obtained through eliminating all the negative conductances g_k's from the circuit in Fig. 1(b), respectively.

III. Reflection-Type Power Amplifier

A. Circuit Configuration

A reflection-type amplifier can be constructed by connecting a circulator to the output port of the ladder structure with the other end shorted (see Fig. 6(a)). In a similar way to the case of a transmission amplifier, the equivalent

[3] Too large N may give rather narrower frequency response.

[4] Actually, the frequency dependence of the g_k value contributes to the frequency response.

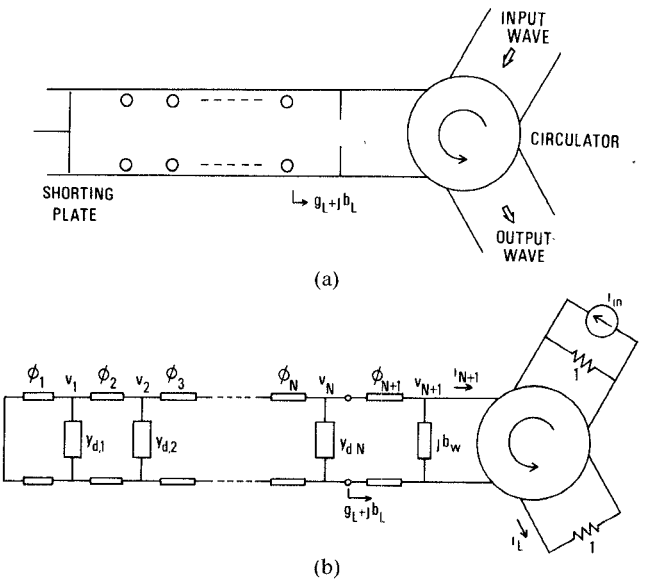

Fig. 6. Reflection-type power amplifier. (a) Construction. (b) Equivalent-circuit representation.

circuit representation is given in Fig. 6(b). ϕ_{N+1} is the electrical length between the Nth mount-pair and the coupling window whose susceptance is denoted by b_w. i_{N+1} and i_L are the currents at the window and at the circulator output.

The circuit equation is written from Fig. 6(b) as

$$b_{tk}V_{k-1}\sin\psi_{k,k-1}+g_kV_k-b_{t,k+1}V_{k+1}\sin\psi_{k+1,k}=V_{in}\cos\psi_{N+1}\cdot\delta_{k,N+1} \quad (24a)$$

$$b_{tk}V_{k-1}\cos\psi_{k,k-1}+b_kV_k+b_{t,k+1}V_{k+1}\cos\psi_{k+1,k}=-V_{in}\sin\psi_{N+1}\cdot\delta_{k,N+1},\qquad k=1,2,\cdots,N+1 \quad (24b)$$

where

$$g_{N+1}=1 \quad (25a)$$

$$b_k=\begin{cases}-\cot\phi_k+b_{pk}-\cot\phi_{k+1}, & 1\leqq k\leqq N\\ -\cot\phi_{N+1}+b_w, & k=N+1\end{cases} \quad (25b)$$

$$b_{tk}=\begin{cases}\operatorname{cosec}\phi_k, & 2\leqq k\leqq N+1\\ 0, & k=1,\ N+2.\end{cases} \quad (25c)$$

Eliminating V_{N+1} and ψ_{N+1} from (24a) and (24b), and using $g_L=b_{t,N+1}^2/(1+b_{N+1}^2)$ and $b_L=-\cot\phi_{N+1}-g_Lb_{N+1}$, we obtain

$$b_{t,N}V_{N-1}\sin\psi_{N,N-1}+(g_N+g_L)V_N=-\sqrt{g_L}\,V_{in}\cos\left\{\psi_N-\cot^{-1}(b_w-\cot\phi_{N+1})\right\} \quad (26a)$$

$$b_{t,N}V_{N-1}\cos\psi_{N,N-1}+(b_N+\cot\phi_{N+1}+b_L)V_N=\sqrt{g_L}\,V_{in}\sin\left\{\psi_N-\cot^{-1}(b_w-\cot\phi_{N+1})\right\}. \quad (26b)$$

B. Perfect Power-Combining Operation

As the load current i_L in Fig. 6(b) is given by $i_L=i_{N+1}+(1/2)i_{in}$ [11], the output power of the reflection amplifier can be expressed, using $i_{N+1}=Y_0v_{N+1}-i_{in}$ and (1) and

(24a), as

$$P_0 = \frac{1}{2Y_0}|i_L|^2 = \frac{1}{8}Y_0 V_{in}^2 - \frac{1}{2}Y_0 \sum_{k=1}^{N} g_k V_k^2. \quad (27)$$

Comparing (27) with (7), we see that the whole input available power $P_{in,a} = Y_0 V_{in}^2/8$ contributes to the output power while it does not in a transmission amplifier. It is apparent from (27) that P_0 reaches the maximum value expressed by (8) when $V_k = V_{k,\mathrm{opt}}$ $(1 \leqq k \leqq N)$; the reflection amplifier is also capable of perfect power combining.

For the perfect power-combining operation of the amplifier in which all the parameters of diode-mount-pairs are equal to each other, we can obtain from (24)

$$(k-1)g_{\mathrm{opt}} = b_{tk}\sin\psi_{k,k-1} \quad (28a)$$

$$\sum_{l=1}^{k-1}(-1)^{k-l}b_l = b_{tk}\cos\psi_{k,k-1}, \qquad 2 \leqq k \leqq N \quad (28b)$$

which is (12) with $P_{in,a}$ omitted. Equations (25), (26), and (28) lead to

$$\left(Ng_{\mathrm{opt}} + g_L\right)^2 + 4g_L g_{\mathrm{opt}}\frac{P_{in,a}}{P_d} = \begin{cases} -(\cot\phi_1 + b_L)^2, & \text{for even } N \\ -(-\cot\phi_1 + b_p + b_L)^2, & \text{for odd } N. \end{cases} \quad (29)$$

When any one of the ϕ_k's $(1 \leqq k \leqq N)$ and either g_L or b_L are given, the remainder can be determined using (28) and (29).

In the case of

$$-\cot\phi_1 = b_L = -b_p/2 \quad (30a)$$

the circuit design for perfect power combining is given from these equations as

$$-\cot\phi_k = \frac{1}{b_p}\left[1 - \left(\frac{b_p}{2}\right)^2 - \left\{(k-1)g_{\mathrm{opt}}\right\}^2\right], \qquad 2 \leqq k \leqq N \quad (30b)$$

and

$$g_{L,\mathrm{opt}} = -g_{\mathrm{opt}}\left(\sqrt{\frac{P_{in,a}}{P_d}} + \sqrt{\frac{P_{in,a}+NP_d}{P_d}}\right)^2. \quad (30c)$$

The $g_{L,\mathrm{opt}}$ value given above is a kind of average of the values of $g_{s,\mathrm{opt}}$ and $g_{L,\mathrm{opt}}$ for the transmission amplifier with the same ladder structure (cf., (10) and (11)). This is because both the input and the output waves travel through the same coupling window in the reflection amplifier. Fig. 2(a) also shows typical ϕ_k and ψ_k values obtained from (30b) and (28).

Defining the normal variables of the traveling waves in the cavity of the reflection amplifier as a_k's and b_k's $(1 \leqq k \leqq N+1)$ in the same way as in the transmission amplifier, we can show that these variables are given by (19) and (20) with $P_{in,a}$ omitted in the amplifier designed by the use of (30) (see Fig. 2(a)). The voltage standing wave in the cavity is also shown in Fig. 2(b).

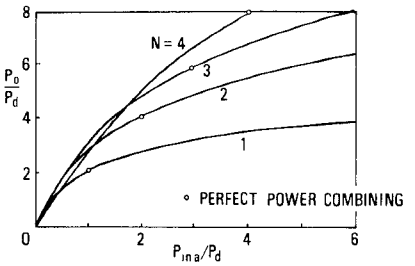

Fig. 7. Output versus input power characteristics of the reflection amplifiers in case of $N = 1 \sim 4$ with $P_{in,0}/P_d = N$ ($g_{\mathrm{opt}} = -0.08$, $b_{p0} = -1.6$).

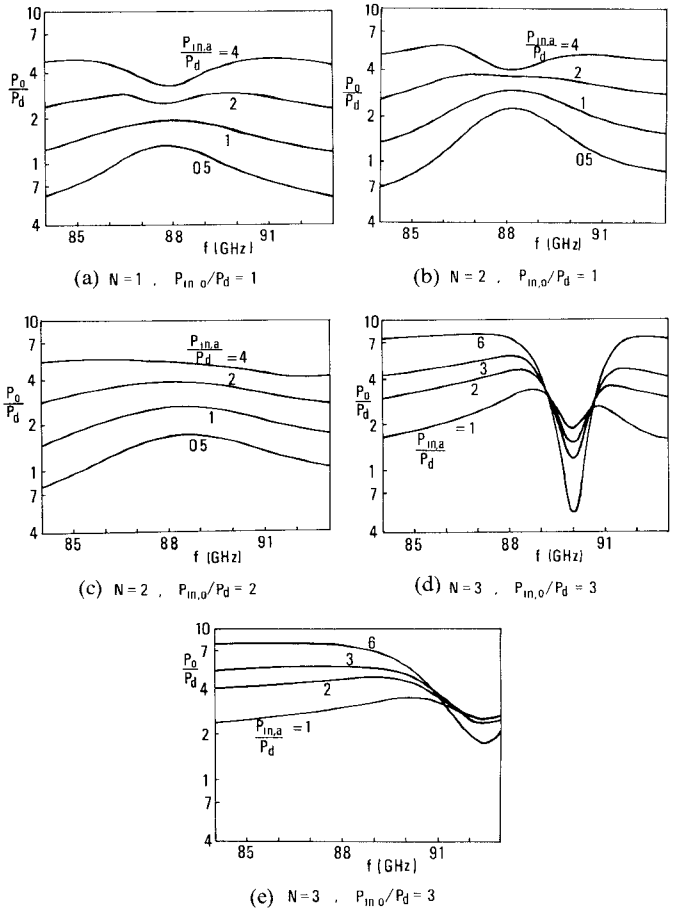

Fig. 8. Frequency responses of the reflection amplifiers. The following data are used: $f_0 = 8.8$ GHz and $g_{\mathrm{opt}} = -0.08$ together with $b_{p0} = -1.6$ and $b_{p1} = 5.1$ for (a)–(d), and $b_{p0} = -0.8$ and $b_{p1} = 2.55$ for (e).

C. Input–Output Characteristic and Frequency Response

Both the output versus input power characteristics and the frequency response in the reflection amplifier are obtained from numerical analysis of (24) in the same way as in the transmission amplifier. The result for the amplifier designed by the use of (30) is given in Figs. 7 and 8, where $g_{L,\mathrm{opt}}$ was determined using (30c) for a specific available input power $P_{in,0}$ at $f = f_0$. Comparing Fig. 7 with Fig. 3, we find that the drop in the combining efficiency η caused by the deviation of $P_{in,a}$ from $P_{in,0}$ is a little larger in the reflection amplifier than in the transmission one. On the other hand, as shown in Figs. 8 and 4, the reflection amplifier has wider and flatter frequency responses for

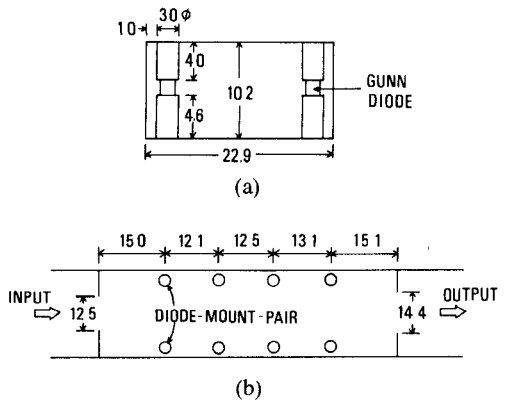

Fig. 9. (a) Configuration of a diode-mount-pair. (b) Typical design of the transmission-type amplifier ($N = 4$, $P_{in,0}/\bar{P}_d = 4$). All dimensions are in millimeters.

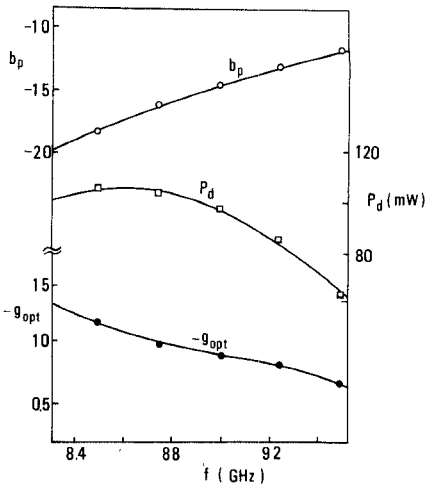

Fig. 10. Typical frequency dependence of g_{opt}, b_p, and P_d of a diode-mount-pair.

$N = 1$ and 2 but narrower responses due to the dip for $N \geqq 3$ than the transmission one. The dip in the frequency response arises from a large standing-wave voltage amplitude at some diode-mount-pair so that the mount-pair has positive conductance near the dip frequency. When a smaller $|b_p|$ is used, the dip frequency becomes more separated from f_0, as seen in Fig. 8(e).

IV. Experiment

Experiments were performed in X-band using Gunn diodes GD511A manufactured by the Nippon Electric Company. The configuration of the basic module with a diode-mount-pair is shown in Fig. 9(a). Table I shows the measured values of g_{opt}, b_p, and P_d when each diode-mount-pair operates as a double-diode oscillator at 8.8 GHz. The typical frequency dependence of these parameters is shown in Fig. 10.

For the transmission-type power amplifiers with N mount-pairs, we determined $g_{s,opt}$, $g_{L,opt}$, b_s, ϕ_k ($2 \leqq k \leqq N$), and b_L by (10), (11), (17), (15′), and (16′), respectively, by the use of the mean measured values in Table I for b_p, g_{opt}, P_d, and specified available input power $P_{in,0}$ for $P_{in,a}$ (the mean value of P_d is denoted as $\bar{P}_d$ in the figures following). Fig. 9(b) shows the design for the typical case of $N = 4$ and $P_{in,0}/P_d = 4$. The amplifiers were constructed near the design obtained in this fashion. Fine adjustments on the source and load using stub-tuners placed behind both the input and the output windows were made so as to maximize the output power for the input power of $P_{in,0}$ at 8.8 GHz. The reflection-type power amplifiers were designed using (30a)–(30c) and constructed in quite a similar way to the transmission-type ones.

The measured results for the output versus input power characteristics and the frequency response are shown in Figs. 11 and 12, respectively. In the case of Fig. 12 (b), (c), and (f), the ladder structures had self-sustained oscillations before introducing an input signal, and they could easily be injection-locked with a locking range of more than 0.6 GHz. Comparing Fig. 11 with Figs. 3 and 7, we can find that the experimental result for the output versus input power characteristics agrees well with the theoretical one

TABLE I

Mount-pair	P_d (mW)	$-g_{opt}$	b_p
No.1	101	0.088	-1.58
No.2	91	0.095	-1.58
No.3	104	0.075	-1.56
No.4	93	0.115	-1.71

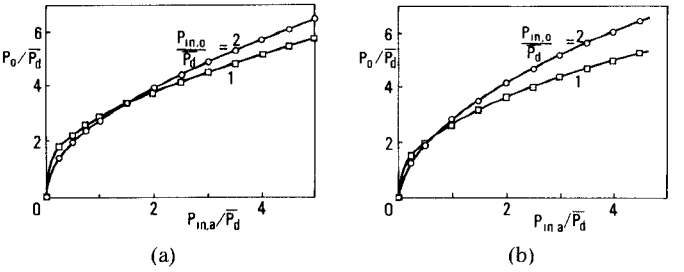

Fig. 11 Experimental result for output versus input power characteristics. (a) Transmission amplifiers ($N = 2$). (b) Reflection amplifiers ($N = 2$).

including perfect power combining. As for the frequency response, comparison of Fig. 12 with Figs. 4 and 8 shows qualitative agreement between the experimental result and the theoretical one. (Note that Figs. 4 and 8 can be applied also for unstable amplifiers as long as they are injection-locked to the input signal.) It is considered that the quantitative difference between the results mainly arise from the differences in frequency dependence of g_{opt} and P_d between the measured and the assumed in the numerical analysis: in the latter, frequency independent values were used both for g_{opt} and P_d.

In order to investigate the usability of the amplifiers for amplification of a PCM–PM input wave, we observed the transient phase response of the amplifiers to a 0-π phase-modulated input signal. The input signal generated using a p-i-n diode modulator had the transition time of 15 ns and the carrier frequency f_0. The measured output phase transi-

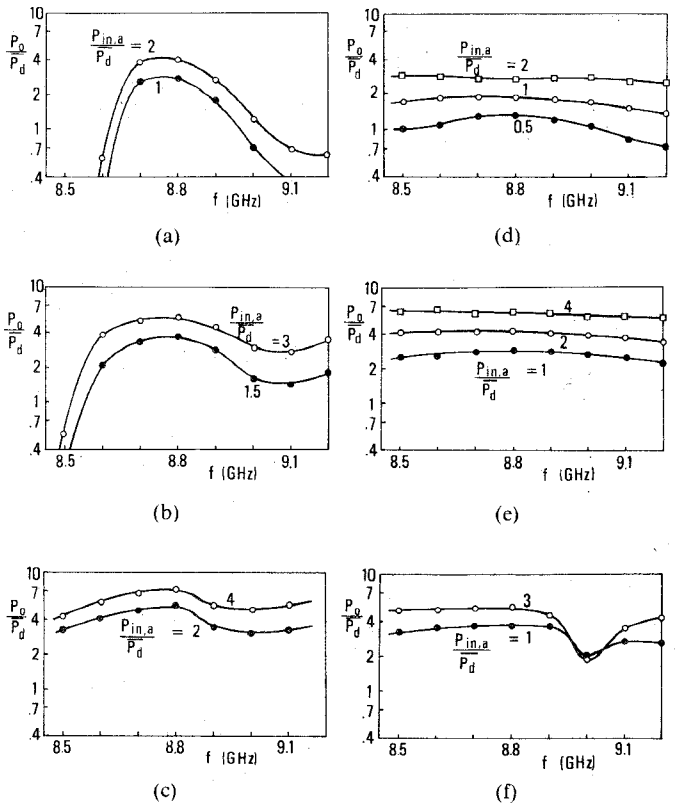

Fig. 12. Experimental result for frequency response. Transmission amplifier: (a) $N=2$, (b) $N=3$, (c) $N=4$. Reflection amplifier: (d) $N=1$, (e) $N=2$, (f) $N=3$. In each case, the design is made for $P_{in,0}/\bar{P}_d = N$.

tion time for every amplifier shown in Fig. 12 was nearly equal to that of the input signal, which shows that the ladder amplifiers have quick response sufficient for practical application.

V. Conclusion

It has been shown that a power amplifier using a multiple-device ladder structure, be it a transmission- or reflection- type, can give the output power equal to the sum of the available powers of each component device plus available input signal power.

Numerical analysis was carried out on the output versus input power characteristics and the frequency response of typical amplifiers with up to four diode-mount-pairs ($N \leqq 4$), whose results were well confirmed by the experiments. It was found that the reflection-type amplifiers with relatively small N and the transmission-type ones with relatively large N exhibit considerably broad frequency response sufficient for practical use. As mentioned in Sections II and III, wide frequency-range response can be brought about by use of smaller absolute values of diode-mount susceptances, that is, by use of diode-mounts closer to the sidewalls of the waveguide. In the experiment, stable amplification was limited to rather small N. In order for the ladder structure of larger N to operate as a stable amplifier, use of the waveguide of reduced height and/or, again, the diode-mounts placed closer to the sidewall is considered to be effective.

Compared with the conventional power amplifier/combiner methods [12], [13], in which input signal is successively divided, amplified and recombined, the multiple-device power amplifier as treated in this paper is considered to be advantageous in its simplicity in construction of amplifier system and, accordingly, in its smaller insertion loss because of no use of the divider/combiner, while it might be less favorable for heat dissipation.

Further detailed and extensive investigations are needed to put the device into practical use.

References

[1] K. Russell, "Microwave power combining techniques," *IEEE Trans. Microwave Theory Tech.*, vol. MTT-27, pp. 472–477, May 1979.

[2] K. Chang and C. Sun, "Millimeter-wave power-combining techniques," *IEEE Trans. Microwave Theory Tech.*, vol. MTT-31, pp. 91–107, Feb. 1983.

[3] K. Fukui and S. Nogi, "Power combining ladder network with many active devices," *IEEE Trans. Microwave Theory Tech.* vol. MTT-28, pp. 1059–1067, Oct. 1980.

[4] K. Fukui and S. Nogi, "A microwave multiple-diode ladder oscillator," *Trans. IECE Japan*, vol. J64-B, pp. 816–823, Aug. 1981.

[5] S. Nogi and K. Fukui, "Optimum design and performance of a microwave ladder oscillator with many diode mount pairs," *IEEE Trans. Microwave Theory Tech.*, vol. MTT-30, pp. 735–743, May 1982.

[6] K. Kurokawa and F. M. Magalhaes, "An *X*-band 20-watt multiple-IMPATT oscillator," *Proc. IEEE*, vol. 59, pp. 102–103, Jan. 1971.

[7] K. Chang and R. L. Ebert, "*W*-band power combiner design," *IEEE Trans. Microwave Theory Tech.*, vol. MTT-28, pp. 295–305, Apr. 1980.

[8] Y.-E. Ma and C. Sun, "1-W millimeter-wave Gunn diode combiner," *IEEE Trans. Microwave Theory Tech.* vol. MTT-28, pp. 1460–1463, Dec. 1980.

[9] A. Materka and S. Mizushina, "A waveguide-cavity multiple-device FET oscillator," *IEEE Trans. Microwave Theory Tech.*, vol. MTT-30, pp. 1237–1241, Aug. 1982.

[10] M. Madihian and S. Mizushina, "A 3m-device cavity-type power combiner," *IEEE Trans. Microwave Theory Tech.*, vol. MTT-31, pp. 731–735, Sept. 1983.

[11] K. Kurokawa, "Injection locking of microwave solid-state oscillators," *Proc. IEEE*, vol. 61, pp. 1386–1410, Oct. 1973.

[12] H. J. Kuno and D. L. English, "Millimeter-wave IMPATT power amplifier/combiner," *IEEE Trans. Microwave Theory Tech.*, vol. MTT-24, pp. 758–767, Nov. 1976.

[13] Y. Tokumitsu, T. Saito, N. Okubo, and K. Kaneko, "A 6-GHz 80-W GaAs FET amplifier with a TM-mode cavity power combiner," *IEEE Trans. Microwave Theory Tech.*, vol. MTT-32, pp. 301–308, 1984.

✠

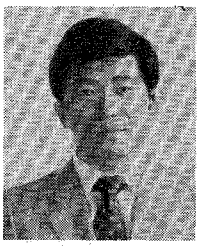

Shigeji Nogi was born in Osaka Prefecture, Japan, on December 26, 1945. He received the B.E., M.E., and D. Eng. degrees in electronics engineering from Kyoto University, Kyoto, Japan, in 1968, 1970, and 1984, respectively.

From 1970 to 1972, he was employed by the Central Research Laboratory, Mitsubishi Electric Corporation, Amagasaki, Japan. In 1972, he joined the Department of Electronics, Okayama University, where he has been engaged in research on microwave active circuits, multimode oscillators, and nonlinear wave propagation.

Dr. Nogi is a member of the Institute of Electronics and Communication Engineers of Japan.

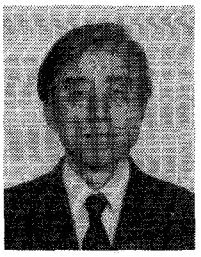

Kiyoshi Fukui (M'75) was born in Tokushima Prefecture, Japan, on January 13, 1930. He received the B.Sc. degree in physics in 1952 and the D. Eng. degree in electronics engineering in 1964, both from Kyoto University, Kyoto, Japan.

From 1958 to 1962, he was a Research Assistant at the Department of Electronics, Kyoto University. From 1962 to 1967, he taught as an Assistant Professor at the Training Institute for Engineering Teachers, Kyoto University. In 1967, he became a Professor of Electronics at the Himeji Institute of Technology, Himeji, Japan. Since 1971, he has been with the Department of Electronics, Okayama University. During 1977–1978, he was on research leave at the University of Wisconsin, Madison. His research interests have been mainly in nonlinear phenomena in electronics such as locking phenomena in oscillators, frequency multiplication by variable capacitance, behavior of multiple-device structures, and nonlinear wave propagation.

Dr. Fukui is a member of the Institute of Electronics and Communication Engineers of Japan and the Physical Society of Japan.

✠

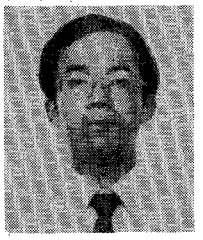

Satoshi Tanaka was born in Okayama Prefecture, Japan, on August 29, 1957. He received the B.E. and M.E. degrees in electronics engineering from Okayama University, Okayama, Japan. The subject of his Master's thesis was microwave power combining.

Since 1982, he has been with Visual Information Systems Development Center of Matsushita Electric Co., Moriguchi, Japan, where he has been engaged in development of home-bus systems.